Supporting Information

Concentration Dependence of Dynamics and Structure among Hydrated Magnesium Ions: An Ultrafast Infrared Study

Samantha T. Hung,[†] Sean A. Roget,[†] Weizhong Zheng,[‡] and Michael D. Fayer[†*]

[†]Department of Chemistry
Stanford University, Stanford, CA 94305, USA
*Phone: (650) 723-4446; Email: fayer@stanford.edu

[‡]State Key Laboratory of Chemical Engineering
East China University of Science and Technology, Shanghai 200237, China

1. Additional Details on Sample Preparation

A. Exothermic Dissolution of $MgCl_2$

Dissolution of $MgCl_2$ is highly exothermic,[1] so heat-resistant vessels that are at least four times the desired solution volumes were used. This was especially important in preventing the solution from bubbling over and splashing while preparing the large volumes (~20 mL per concentration) of solutions needed for measuring the kinematic viscosity.

B. Probe Concentration

It is important to use a low enough concentration of the vibrational probe to prevent the probe from interfering with the measurement of the true solution dynamics. It is also desirable to use a high enough concentration for adequate signal-to-noise ratio. In this study, KSeCN was added at 0.25 molal concentration. Halving the probe concentration produced identical dynamics, as was previously observed for $SeCN^-$ dynamics in pure D_2O,[2] so the 0.25 m concentration was used to increase signal strength.

C. Deuterated Water vs Normal Water

Deuterated water (D_2O) was used in this study instead of H_2O since the combination band in H_2O spectrally overlaps with the CN stretch of $SeCN^-$ and facilitates vibrational relaxation, resulting in CN lifetimes that are almost ten times shorter (~4 ps)[3] than the lifetimes in D_2O (~20-40ps). The longer lifetimes in D_2O facilitate the measurement of the relatively long dynamics at high concentrations (e.g., >200 ps for the Mg^{2+} associated rotational dynamics in 1-12 solution).

2. Solution Properties

Table S1. Concentration, Density, and Viscosity of $MgCl_2$ in D_2O at 22°C[a]

Concentration (mole ratio)	Mole Fraction	Molality (m)	Molarity (M)	Density (g/mL)	η (cP)
1-12	0.077	4.2	4.1	1.366 ± 0.001	8.08 ± 0.01
1-16	0.059	3.1	3.2	1.3123 ± 0.0004	4.66 ± 0.01
1-20	0.048	2.5	2.6	1.2781 ± 0.0002	3.47 ± 0.01
1-30	0.032	1.7	1.8	1.2252 ± 0.0005	2.38 ± 0.01
1-40	0.024	1.2	1.3	1.1974 ± 0.0001	1.97 ± 0.01
1-100	0.010	0.5	0.5	1.1428 ± 0.0003	1.46 ± 0.01
D_2O	-	-	-	1.1037 ± 0.0001[b]	1.18 ± 0.01[c]

[a]Densities and viscosities were measured at 22 °C in the same room where the spectroscopic measurements were made. D_2O used is 99.9 mole % D.
[b]Compare to 1.1053 g/mL at 20°C for D_2O from the CRC Handbook.[4]
[c]Compare to the interpolated value of 1.187 cP at 22°C for D_2O with 100 mole % D from literature (National Bureau of Standards).[5]

3. Isotropic Pump-Probe Signals *P*(*t*)

A. Long Time Offset (Mg^{2+} Associated Peak)

The entire CN absorption (both peaks) is on the tail of a strong and broad OD band centered ~500 cm^{-1} to the blue of the CN transitions, and the OD absorption underneath the bluer Mg^{2+} associated $SeCN^-$ frequencies is not negligible. Thus, even in samples with no $SeCN^-$, a background signal grows in to give the longtime offset. The offset is caused by a small temperature increase arising from the solvent absorption and rapid relaxation depositing heat in the sample. Background subtraction was performed on data collected with and without the $SeCN^-$ probe to isolate the dynamics associated with the $SeCN^-$ probe. A simpler approach is to subtract the long time offset measured at very long time delays (over an order of magnitude greater than the lifetime). This method yielded identical results within error, but with improved data quality, which facilitates analysis of the slow rotational dynamics.

B. $P(t)$ Decays for D_2O and Mg^{2+} Associated $SeCN^-$

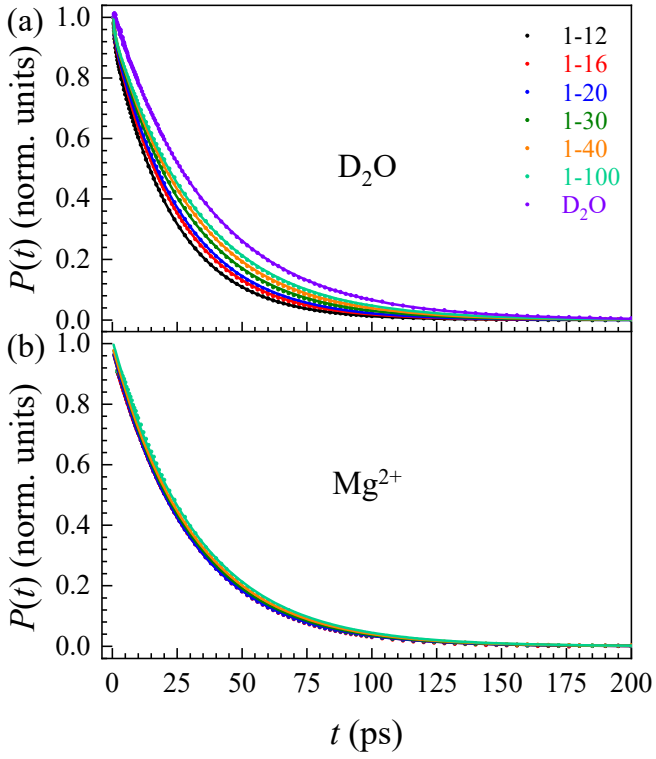

Figure S1. Measured isotropic pump-probe $P(t)$ decays of $SeCN^-$ in D_2O solutions of varying $MgCl_2$ concentrations and in pure D_2O. (a) The solid curves are biexponential fits to the data for the D_2O peak. The final time constants correspond to the $SeCN^-$ CN stretch vibrational lifetimes. (b) The solid curves are single exponential fits to the data for the Mg^{2+} peak. The time constants are the vibrational lifetimes.

C. Vibrational Lifetime of Mg^{2+} Associated $SeCN^-$

Although the Mg^{2+} 0-1 transition overlaps with the broad D_2O 0-1 band, there is no discernible complication. At high salt concentrations where the D_2O contribution is minimal, the ~20 ps lifetime of the free peak could not be resolved from the $P(t)$ traces, and the ~30 ps Mg^{2+} lifetime dominates. At low concentrations, the D_2O and Mg^{2+} lifetimes are identical within error (~30 ps), making any D_2O contribution irrelevant. Thus, it was reasonable to assume the $P(t)$ at the Mg^{2+} frequencies give the Mg^{2+} lifetimes.

4. Anisotropy Decays $r(t)$

A. Two-Component Fits (Mg^{2+} Associated Peak)

In analyzing the $r(t)$ decays measured at the Mg^{2+} frequencies, the two contributing D_2O and Mg^{2+} ensembles can be separated using a two-component model:[6]

$$r(t) = 0.4\frac{aP_1(t)C_2^1(t) + (1-a)P_2(t)C_2^2(t)}{aP_1(t) + (1-a)P_2(t)}, \tag{S1}$$

where $P_i(t)$ represents the vibrational lifetime decay and $C_2^i(t)$ the orientational correlation function of the i^{th} species. The weighting factor a reflects the relative populations of the two species. Here, the $P(t)$ are modeled as single exponential functions and $C_2(t)$ as multiexponential functions. Given that there is no frequency dependence for the D_2O contribution, $P_1(t)$ and $C_2^1(t)$ can be fixed to the already determined D_2O parameters. As described above, the lifetime of the Mg^{2+} peak is not appreciably altered by the D_2O peak. Accordingly, $P_2(t)$ is given by $P(t)$ directly measured at the Mg^{2+} frequencies. However, a lack of two components in the Mg^{2+} $P(t)$ precludes determination of the relative population factor a.

Given that the D_2O dynamics (main text Figure 3a) are much faster than the Mg^{2+} dynamics (Figure 3b) and the long time components of direct fits to the Mg^{2+} $r(t)$ decays do not vary appreciably with frequency, the Mg^{2+} $C_2^2(t)$ was assumed to be frequency independent to constrain the fits. This implies that the frequency dependence of the measured $r(t)$ is solely due to the varying contribution of the faster D_2O dynamics at early times, which is reasonable given that the faster decays are at redder frequencies where there is greater D_2O contribution. The Mg^{2+} $C_2^2(t)$ long time component (amplitude and time scale) was first determined by fitting the long time data points for frequencies in a 10 cm^{-1} range by fixing the D_2O contributions ($P_1(t)$ and long time $C_2^1(t)$ amplitude and time scale). Then, the full time range was fit with the newly determined long time component fixed, giving the shorter time component. Figure S2 shows the two-component fits to the 1-20 mole ratio data over a range of frequencies associated with the Mg^{2+} peak.

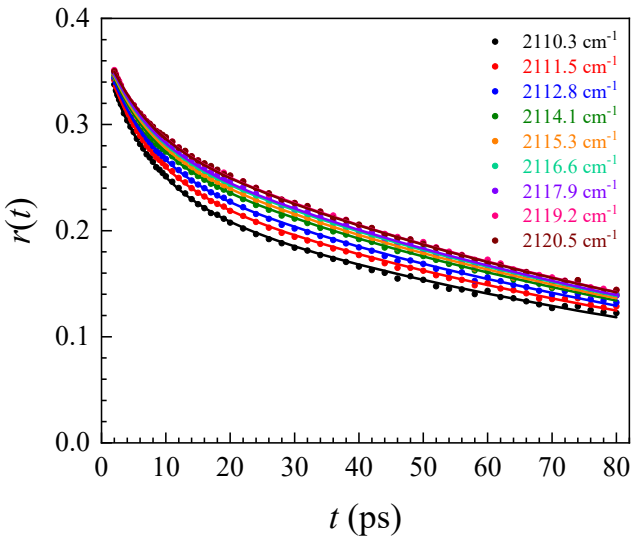

Figure S2. Measured rotational anisotropy $r(t)$ decays of $SeCN^-$ associated with Mg^{2+} in 1-20 $MgCl_2$ D_2O solution over a range of 10 cm^{-1}. The solid curves are two-component fits described by Eq. S1.

Table S2. Orientational Relaxation Parameters (Mg^{2+} Associated Peak)[a]

Sample	A_1	t_1 (ps)	A_2	t_2 (ps)
1-12	0.062 ± 0.006	10 ± 2	0.318 ± 0.006	200 ± 19
1-16	0.074 ± 0.005	8 ± 1	0.298 ± 0.005	148 ± 11
1-20	0.095 ± 0.001	7.4 ± 0.7	0.275 ± 0.004	120 ± 10
1-30	0.108 ± 0.005	5.0 ± 0.5	0.27 ± 0.01	87 ± 8
1-40	0.14 ± 0.02	4.5 ± 0.1	0.23 ± 0.01	73 ± 3
1-100	0.198 ± 0.005	3.3 ± 0.3	0.18 ± 0.01	51 ± 5

[a]Biexponential fit parameters to the anisotropy (averaged over 10 cm^{-1} around the center frequency) for $SeCN^-$ associated with Mg^{2+} in D_2O solutions of varying $MgCl_2$ concentrations. This is without considering the contribution from $SeCN^-$ associated with D_2O. The A_i and t_i are the amplitude and time constant of the ith component.

The resulting biexponential parameters for the Mg^{2+} peak from the two-component fits (main text Table 2) are similar to direct (assuming no D_2O contribution) fits to the data (Table S2), with almost no change in the long time scale. Considering that the long time scale is much longer for Mg^{2+}, it is reasonable that it is mostly unaffected by the fast D_2O contribution, confirming the origin of seemingly frequency dependent anisotropies to varying contribution of the D_2O dynamics. The parameters a, or fraction of D_2O dynamics, at different frequencies match the relative contributions of the D_2O 0-1 band under the Mg^{2+} 0-1 band at corresponding

frequencies when early time pump probe spectra were fit with four Gaussians modeling the two 0-1 and two 1-2 transitions.

B. Wobbling-in-a-Cone Analysis

The orientational correlation function $C_2(t)$ is modeled with ultrafast inertial motions, diffusive time constant(s) τ_c for restricted angular diffusion ("wobbling" motions), and a final time constant τ_m for complete orientational randomization:[7]

$$C_2(t) = T^2\left\{S^2 + \left(1 - S^2\right)\exp\left[-t/\tau_{c1}\right]\right\}\left\{R^2 + \left(1 - R^2\right)\exp\left[-t/\tau_{c2}\right]\right\}\exp\left[-t/\tau_m\right] \qquad \text{(S2)}$$

The square of the generalized order parameter, T^2, gives the amplitude of the inertial decay that is too fast to contribute to the observed dynamics and does not have an associated time constant. The general form of the squared order parameters T^2, S^2, and R^2 is:

$$Q^2 = \left[\frac{1}{2}\cos\theta_c\left(1 + \cos\theta_c\right)\right]^2, \qquad \text{(S3)}$$

where θ_c is the half angle of the angular cone explored by the CN transition dipole. For a triexponential decay, there are two wobbling periods, the faster of which describes more restricted wobbling motion with time constant τ_{c1} and smaller cone angle θ_{c1}. For a biexponential decay, this is the sole wobbling period. If there were no additional decay processes, the corresponding part of $C_2(t)$ in Eq. S2 decays to a plateau with value S^2. As the solvent structure evolves, constraints on angular displacement are relaxed and the CN dipole explores greater angular space. For a triexponential decay, the second wobbling process is described by cone angle θ_{c2} and time constant τ_{c2}, and in the absence of further orientational relaxations, $C_2(t)$ then decays to R^2, where $R^2 < S^2$, reflecting greater loss in orientational correlation. Relaxation of all angular restrictions results in complete orientational randomization, and $C_2(t)$ decays to zero with time constant τ_m.[8-10] The generalized order parameters T, S, and R were determined from fits to the data with Eq. S2, and using Eq. S3, the inertial cone half angle θ_{in} and the diffusive cone half angles θ_{c1} and θ_{c2} were calculated from the corresponding parameters. The total order parameter $Q_{tot} = TRS$ gives the total cone half angle θ_{tot}, which describes the entire range of angular space sampled over all periods of restricted orientational diffusion. The cone half angles and time constants are tabulated in Table S3.

Table S3. Wobbling Analysis Parameters[a]

Sample		θ_{in} (º)	θ_{c1} (º)	θ_{c2} (º)	θ_{tot} (º)	τ_{c1} (ps)	τ_{c2} (ps)	τ_m (ps)
D_2O	1-12	16.1 ± 0.1	14.3 ± 0.2	44 ± 2	48 ± 1	3.1 ± 0.2	16.1 ± 0.1	67 ± 8
	1-16	16.5 ± 0.6	18 ± 1	53 ± 2	57 ± 2	2.9 ± 0.1	16.5 ± 0.6	54 ± 2
	1-20	16.6 ± 0.1	17 ± 3	56 ± 2	60 ± 2	2.4 ± 0.6	16.6 ± 0.1	39 ± 5
	1-30	17 ± 1	15 ± 3	51 ± 2	55 ± 2	2.1 ± 0.5	17 ± 1	16 ± 2
	1-40	17 ± 1	16 ± 1	54 ± 6	58 ± 5	2.6 ± 0.8	17 ± 1	14 ± 3
	1-100	17 ± 1	9 ± 3	48 ± 9	51 ± 8	1.3 ± 0.6	17 ± 1	8.3 ± 1.4
	D_2O[2]	11.3 ± 0.1	21.5 ± 0.4	-	24.2 ± 0.3	2.0 ± 0.1	-	4.5 ± 0.1
Mg^{2+}	1-12	11 ± 1	20 ± 1	-	22 ± 1	16 ± 3	-	226 ± 27
	1-16	12 ± 1	20 ± 3	-	23 ± 3	8 ± 3	-	148 ± 17
	1-20	12 ± 1	23.3 ± 0.4	-	26 ± 1	8 ± 1	-	119 ± 9
	1-30	8 ± 2	22 ± 3	-	24 ± 4	3.6 ± 0.4	-	83 ± 4
	1-40	6 ± 5	22 ± 3	-	23 ± 4	3 ± 1	-	78 ± 7
	1-100	1 ± 2	34 ± 2	-	34 ± 2	3.0 ± 0.1	-	59 ± 8

[a]See text for parameter descriptions.

C. Deviations from SED Behavior

The log-log plot in the main text (Figure 4a) displays fits to the data with unity slope, in accordance with the standard Stokes-Einstein-Debye (SED) model[11-13] and Eq. 3. The fit to the Mg^{2+} associated data is reasonable but the fit to the D_2O associated data has larger residuals. To see if better fits can be achieved and explained, we begin by exploring the possibility of fractional SED (FSED) behavior, meaning the complete orientational relaxation time τ_m is proportional to the power of the ratio of the bulk dynamic viscosity η of the solvent to the absolute temperature T: $\tau_m = (\eta/T)^x \times (V/k_B)$.[14-16] The log-log form of this equation gives:

$$\log(\tau_m) = x \cdot \log\left(\frac{\eta}{T}\right) + \log\left(\frac{V}{k_B}\right). \quad \text{(S4)}$$

Shown in Figure S3 are linear fits to the experimental data of $SeCN^-$ in aqueous $MgCl_2$ D_2O solutions of varying concentrations. The solid black lines are fits with slopes fixed to one (i.e., standard SED behavior).

In Figure S3a, the dashed red line is a linear fit to the Mg^{2+} associated peak and has a slope of ~0.8. The fit is excellent, but the extracted volume V of the rotator from this fit would be ~10 Å^3 for Mg^{2+} associated species. Considering that the $SeCN^-$ probe has a volume of ~50 Å^3, 10 Å^3 is unreasonable. The fit with fixed unity slope to the Mg^{2+} data gives a volume of 141 Å^3, which is comparable to the volume of the vibrational probe along with the Mg^{2+} cation and coordinated waters (149 Å^3). It is possible to still obtain this volume and the FSED slope of 0.8 (i.e., the excellent fit) if we account for the boundary condition factor C, which is equal to 0 for a spherical rotator with slip boundary conditions and equal to 1 for any rotator with stick boundary conditions.[17] The boundary condition factor can be included as a log(C) term, with C ~0.1, suggesting slip boundary conditions. The shape factor f can also be included (total correction term being log(fC)), and f increases from unity for increasing deviation from sphericity.[18]

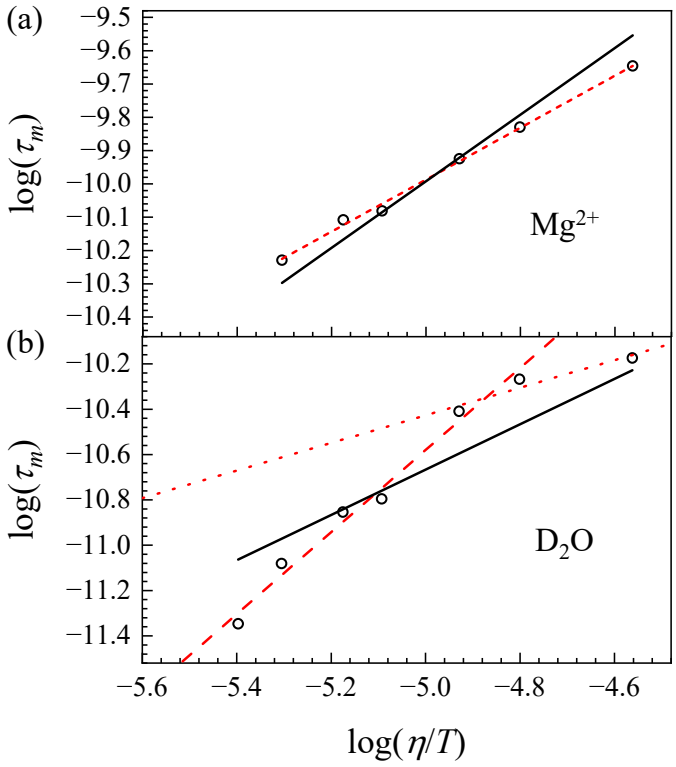

Figure S3. Log-log plots of the orientational relaxation time τ_m (in seconds) versus the ratio η/T of the viscosity (in Pa·s) to the temperature (fixed at ~295 K) for $SeCN^-$ in $MgCl_2$ solutions. The solid black lines are fits with fixed unity slope through all of the corresponding data points, in accordance to the SED model. The dashed red line in (a) has a slope of ~0.8. The dashed and dotted red lines in (b) fitting different concentration ranges for the D_2O associated peak have different slopes.

In Figure S3b, the SED fit with unity slope (solid black line) for the D_2O associated peak gives a volume of ~30 Å^3, which is smaller than the ~50 Å^3 for an $SeCN^-$ anion. However, the data can be fit better with two lines of different slopes (i.e., different FSED behavior), and the abrupt change in slope may reflect changes in the solvent structure. The dashed red line fits the data from pure D_2O to 1-30 mole ratio concentrations and the dotted red line for solutions with concentrations at and above 1-20. They fit the data well with slopes of 1.8 and 0.6, respectively, but produce unphysical volumes either on the scale of hundreds of thousands of Å^3 or almost zero.

It should be noted that in the study of $SeCN^-$ in pure D_2O, it was proposed that $SeCN^-$ exhibited near Debye diffusion, as the ratio of the correlation times for $C_1(t)$ to $C_2(t)$ was just under the expected value of 3 (~2.6-2.8).[2] However, the hydrodynamic volume of 15 Å^3 extracted from the τ_m is also smaller than expected for a 50 Å^3 $SeCN^-$. Mechanistically, $SeCN^-$ reorientation probably requires breaking and forming multiple H-bonds (i.e., "jumps"), which may result in deviations from SED predictions. As for FSED behavior, while variation of the x value (the power law dependence of η/T in the modified SED equation or the non unity slope in the log-log plot) allows for better fits to the data, it is not necessarily a reasonable assumption. FSED behavior is usually observed in liquids at temperatures below the glass transition temperature T_g, and SED behavior at $T \geq 1.5\ T_g$.[19-20] Note that T_g is ~138 K for H_2O and 173 K for concentrated $MgCl_2$ solution.[21] The experiments in this study were performed at ~300 K. It is not impossible for FSED behavior to be observed above T_g, as shown in a molecular dynamics study of H_2O (258 K) and D_2O (265 K) at atmospheric pressures.[22] However, given that the SED fits are reasonable given experimental errors and possibly small deviations due to non-ideal Debye diffusion behavior and correction factors, the important conclusion is that the cation associated probe molecule reorients much more slowly than the water associated probe molecule in the same solution of a single viscosity.

5. Spectral Diffusion

A. Separation of Different $SeCN^-$ Peaks

The 2D spectra of the nitrile stretch of the $SeCN^-$ in $MgCl_2$ solutions has two overlapping absorption bands from D_2O-$SeCN^-$ and Mg^{2+}-$SeCN^-$ interactions. Typically, spectral diffusion dynamics are extracted from the T_w-dependent spectra of a single $SeCN^-$ ensemble using the

CLS ω_m method. This involves connecting the maximum peak centers of slices of the 2D lineshape about the ω_m axis and determining the slope of the generated center line at each T_w. However, when the two ensembles in the 2D spectra overlap, the center position of the species of interest is obscured due to contributions from the other band. A number of methods have been devised to accurately determine the spectral diffusion dynamics of distinct species in the spectra.[23-25] In this section, the separation of the two species in the $MgCl_2$ solutions to obtain spectral diffusion dynamics following a general method previously described in detail[25] is discussed.

Each type of $SeCN^-$ interaction in the $MgCl_2$ solutions contributes a 0-1 transition and an oppositely signed 1-2 transition to the 2D spectra, resulting in four bands. These four bands were modeled using 2D Gaussian line shapes. A single 2D Gaussian has six parameters: center position and widths in ω_m and ω_τ, the tilt, and the peak amplitude. Least squares fitting was performed using a nonlinear solver in MATLAB 2014b. Many parameters can be constrained by the relationship between the 0-1 and 1-2 transitions of each species. The center position about ω_τ, the widths, and the tilt are shared between the 0-1 and 1-2 transitions. Additionally, the center positions about ω_m and ω_τ are equivalent for the 0-1 transition and identical to the center position of the linear absorption spectra. These can be fixed based on the linear spectra but are bounded to account for experimental deviation. The center position about ω_m is different for the 1-2 transition because of the anharmonicity but can be bounded based on the anharmonicity at early T_w periods.

Examples of fits to the experimental data and the residuals are shown in Figure S4 for the 1-12 concentration, at early and long T_w periods (first and second rows). The data is adequately captured by this model. Once each band is modeled accurately through the fits, each ensemble contributing to the 2D spectra can be isolated by subtracting the Gaussians corresponding to the interfering ensemble from the experimental data, leaving only the desired ensemble. Then, the CLS ω_m method can be performed on the 0-1 transition of the isolated ensemble to extract the spectral diffusion dynamics. Isolated 2D spectra of the Mg^{2+} and D_2O peaks are shown at early and long T_w periods for $MgCl_2$ solution in Figure S5. Some residuals appear in the 2D spectra where there were formerly another ensemble. However, since the CLS ω_m method is done around the very center of the 0-1 transition, the residual features have no impact on the observable.

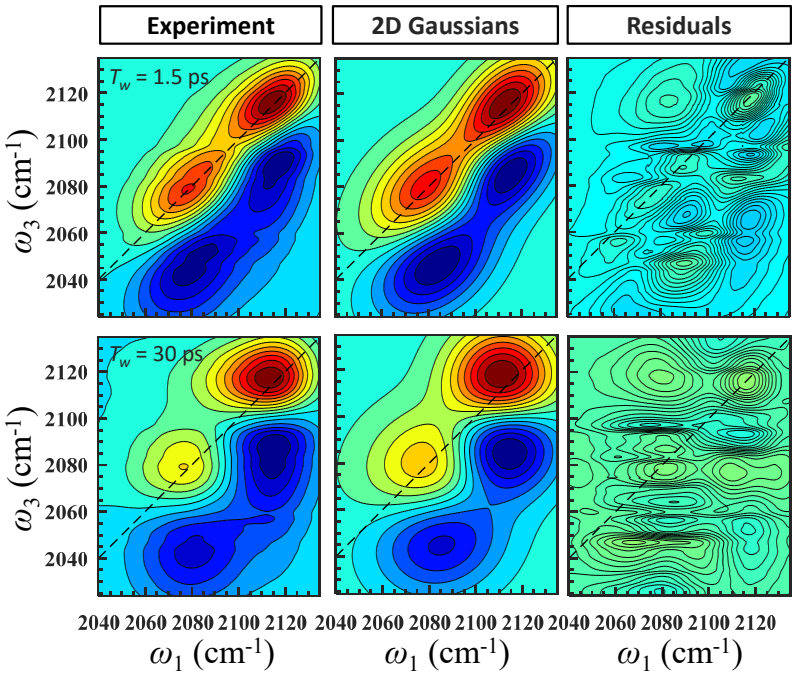

Figure S4. In the leftmost column are experimental 2D IR spectra of the CN stretch of $SeCN^-$ in 1-12 $MgCl_2$ D_2O solutions at time delays T_w = 1.5 and 30 ps. In the middle column are corresponding 2D spectra generated from a sum of four 2D Gaussians, and in the rightmost column are the residuals.

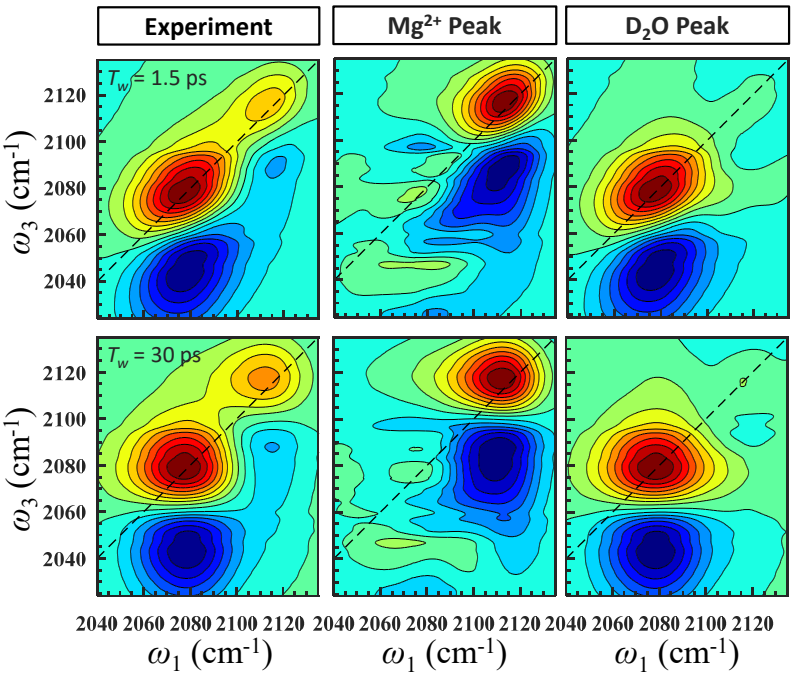

Figure S5. In the leftmost column are experimental 2D IR spectra of the CN stretch of $SeCN^-$ in 1-20 $MgCl_2$ D_2O solutions at time delays T_w = 1.5 and 30 ps. The Mg^{2+} 0-1 and 1-2 transitions in the middle column are isolated by subtracting the 2D Gaussian approximations of the D_2O 0-1 and 1-2 transitions, and vice versa for the D_2O peaks in the rightmost column.

B. Reorientation-Induced Spectral Diffusion (RISD)

The parallel and perpendicular 2D spectra produce different CLS(T_w) decay curves when there are contributions from reorientation-induced spectral diffusion (RISD), which occurs when probe molecules rotate on a time scale comparable to the variation of the solvent electric field. Fast rotation allows a probe to sample structural configurations faster than via changes in its interactions with the solvent as the solvent structure fluctuates. RISD proceeds through the first-order effect for probe molecules with a permanent dipole moment, such as $SeCN^-$.[26-28] The effects obscure the true solvent structural fluctuations, termed structural spectral diffusion (SSD), and are usually non-negligible when the SSD is much slower than the rotation, resulting in deceptively fast CLS decays.

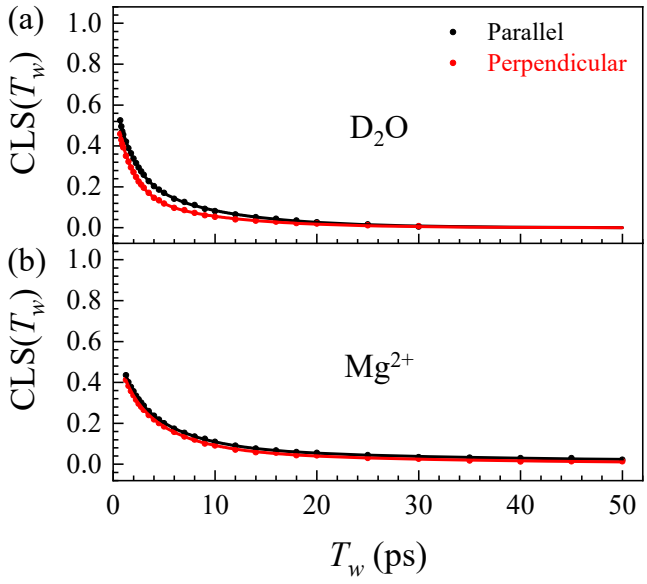

Figure S6. Parallel and perpendicular CLS(T_w) decays (spectral diffusion) of the CN stretch of $SeCN^-$ in 1-16 $MgCl_2$ D_2O solutions for (a) the D_2O associated and (b) the Mg^{2+} associated peaks. The solid curves are multiexponential fits to the data.

For $SeCN^-$ in pure D_2O, the effects of RISD are negligible, with the CLS fit parameters for the parallel and perpendicular decays being within error of each other.[2] This is also the case here with the $MgCl_2$ D_2O solutions, with little difference between the parallel and perpendicular decays for the D_2O associated $SeCN^-$ peak (Figure S6a). The differences are even smaller for the Mg^{2+} associated $SeCN^-$ peak (Figure S6b). These observations are in accord with the fact that the reorientation time scales (main text Table 2) are longer than spectral diffusion (Tables 3 and S4).

For the 1-16 mole ratio shown in Figure S6, the D_2O peak has anisotropy time scales t_2 = 11.4 ps and t_3 = 54 ps, whose amplitudes make up ~90% of the decay, whereas the CLS has over half of its amplitude in the much faster 1.4 ps time scale. For the Mg^{2+} peak, the differences are even larger as the majority of the anisotropy decay is in the 148 ps time scale, and even the slowest CLS time scale is only 29 ps. Furthermore, the anisotropy represents $C_2(t)$, the second order orientational correlation function, which when modeled with a single exponential is a factor of three faster than $C_1(t)$, the dominant term in RISD. Hence, RISD effects should be small. The CLS and FFCF presented were thus directly extracted from the isotropic 2D spectra constructed from the parallel and perpendicular 2D IR data.

C. CLS Parameters

Table S4. CLS Parameters[a]

Sample		A_1	t_1 (ps)	A_2	t_2 (ps)	A_3	t_3 (ps)
D_2O	1-12						
	1-16	0.42 ± 0.01	1.4 ± 0.2	0.25 ± 0.04	8 ± 1		
	1-20	0.43 ± 0.02	1.1 ± 0.1	0.23 ± 0.04	6 ± 1		
	1-30	0.49 ± 0.02	1.2 ± 0.1	0.13 ± 0.02	7 ± 1		
	1-40	0.48 ± 0.03	1.1 ± 0.1	0.11 ± 0.01	6 ± 1		
	1-100	0.47 ± 0.03	0.9 ± 0.2	0.12 ± 0.05	3 ± 1		
	D_2O[2]	0.25 ± 0.03	0.6 ± 0.1	0.31 ± 0.04	1.4 ± 0.2		
Mg^{2+}	1-12	0.20 ± 0.01	1.5 ± 0.1	0.37 ± 0.01	5.4 ± 0.2	0.11 ± 0.03	34 ± 1
	1-16	0.24 ± 0.03	1.2 ± 0.2	0.34 ± 0.01	4.8 ± 0.5	0.08 ± 0.04	29 ± 4
	1-20	0.22 ± 0.03	1.3 ± 0.3	0.31 ± 0.03	3.9 ± 0.2	0.07 ± 0.02	21 ± 5
	1-30	0.25 ± 0.03	1.2 ± 0.3	0.25 ± 0.04	4.0 ± 0.2	0.04 ± 0.01	13 ± 3
	1-40	0.22 ± 0.02	1.5 ± 0.3	0.20 ± 0.03	4.8 ± 0.5	-	-
	1-100						

[a]Multiexponential fit parameters to the CLS for $SeCN^-$ associated with D_2O (top half of table) and with Mg^{2+} (bottom half of the table) in aqueous solutions with varying concentrations of $MgCl_2$. The A_i and t_i are the amplitude and time constant of the ith component.

References

1. Chmarzyński, A. Differential Enthalpies of Solution of $LiCl \cdot H_2O$, NaCl, KCl, $MgCl_2 \cdot 6H_2O$, $CaCl_2 \cdot 6H_2O$, and $BaCl_2 \cdot 2H_2O$ in Water at 298.15 K, near the Saturation Concentration. *J. Therm. Anal.* **1995,** *45* 791-798.
2. Yamada, S. A.; Thompson, W. H.; Fayer, M. D. Water-Anion Hydrogen Bonding Dynamics: Ultrafast IR Experiments and Simulations. *J. Chem. Phys.* **2017,** *146* 234501.
3. Lenchenkov, V.; She, C.; Lian, T. Vibrational Relaxation of CN Stretch of Pseudo-Halide Anions (OCN^-, SCN^-, and $SeCN^-$) in Polar Solvents. *J. Phys. Chem. B* **2006,** *110* 19990-19997.
4. Properties of Saturated Liquid D_2O as a Function of Temperature. CRC Press: 2022.
5. Hardy, R. C.; Cottington, R. L. Viscosity of Deuterium Oxide and Water in the Range 5 to 125 C. *J. Res. Natl. Bur. Stand* **1949,** *42* 573.
6. Roget, S. A.; Kramer, P. L.; Thomaz, J. E.; Fayer, M. D. Bulk-Like and Interfacial Water Dynamics in Nafion Fuel Cell Membranes Investigated with Ultrafast Nonlinear IR Spectroscopy. *J. Phys. Chem. B* **2019,** *123* 9408-9417.
7. Kramer, P. L.; Giammanco, C. H.; Fayer, M. D. Dynamics of Water, Methanol, and Ethanol in a Room Temperature Ionic Liquid. *J. Chem. Phys.* **2015,** *142* 212408.
8. Tokmakoff, A. Orientational Correlation Functions and Polarization Selectivity for Nonlinear Spectroscopy of Isotropic Media. I. Third Order. *J. Chem. Phys.* **1996,** *105* 1-12.
9. Tao, T. Time‐Dependent Fluorescence Depolarization and Brownian Rotational Diffusion Coefficients of Macromolecules. *Biopolymers* **1969,** *8* 609-632.
10. Debye, P. J. W., *Polar Molecules*. Dover: 1929.
11. Sension, R. J.; Hochstrasser, R. M. Comment On: Rotational Friction Coefficients for Ellipsoids and Chemical Molecules with Slip Boundary Conditions. *J. Chem. Phys.* **1993,** *98* 2490-2490.
12. Youngren, G.; Acrivos, A. Rotational Friction Coefficients for Ellipsoids and Chemical Molecules with the Slip Boundary Condition. *J. Chem. Phys.* **1975,** *63* 3846-3848.
13. Moog, R.; Ediger, M.; Boxer, S.; Fayer, M. Viscosity Dependence of the Rotational Reorientation of Rhodamine B in Mono-and Polyalcohols. Picosecond Transient Grating Experiments. *J. Phys. Chem.* **1982,** *86* 4694-4700.
14. Hayduk, W.; Cheng, S. Review of Relation between Diffusivity and Solvent Viscosity in Dilute Liquid Solutions. *Chem. Eng. Sci.* **1971,** *26* 635-646.

15. Evans, D.; Tominaga, T.; Davis, H. Tracer Diffusion in Polyatomic Liquids. *J. Chem. Phys.* **1981,** *74* 1298-1305.

16. Nishiyama, Y.; Fukuda, M.; Terazima, M.; Kimura, Y. Study of the Translational Diffusion of the Benzophenone Ketyl Radical in Comparison with Stable Molecules in Room Temperature Ionic Liquids by Transient Grating Spectroscopy. *J. Chem. Phys.* **2008,** *128* 164514.

17. Hu, C. M.; Zwanzig, R. Rotational Friction Coefficients for Spheroids with the Slipping Boundary Condition. *J. Chem. Phys.* **1974,** *60* 4354-4357.

18. Perrin, F. Mouvement Brownien D'un Ellipsoide-I. Dispersion Diélectrique Pour Des Molécules Ellipsoidales. *J. Phys. Radium* **1934,** *5* 497-511.

19. Mazza, M. G.; Giovambattista, N.; Stanley, H. E.; Starr, F. W. Connection of Translational and Rotational Dynamical Heterogeneities with the Breakdown of the Stokes-Einstein and Stokes-Einstein-Debye Relations in Water. *Phys. Rev. E* **2007,** *76* 031203.

20. Becker, S. R.; Poole, P. H.; Starr, F. W. Fractional Stokes-Einstein and Debye-Stokes-Einstein Relations in a Network-Forming Liquid. *Phys. Rev. Lett.* **2006,** *97* 055901.

21. Angell, C.; Sare, E. Glass‐Forming Composition Regions and Glass Transition Temperatures for Aqueous Electrolyte Solutions. *J. Chem. Phys.* **1970,** *52* 1058-1068.

22. Harris, K. R. The Fractional Stokes–Einstein Equation: Application to Lennard-Jones, Molecular, and Ionic Liquids. *J. Chem. Phys.* **2009,** *131* 054503.

23. Fenn, E. E.; Fayer, M. Extracting 2D IR Frequency-Frequency Correlation Functions from Two Component Systems. *J. Chem. Phys.* **2011,** *135* 074502.

24. Giammanco, C. H.; Kramer, P. L.; Fayer, M. D. Dynamics of Dihydrogen Bonding in Aqueous Solutions of Sodium Borohydride. *J. Phys. Chem. B* **2015,** *119* 3546-3559.

25. Yuan, R.; Fayer, M. D. Dynamics of Water Molecules and Ions in Concentrated Lithium Chloride Solutions Probed with Ultrafast 2D IR Spectroscopy. *J. Phys. Chem. B* **2019,** *123* 7628-7639.

26. Giammanco, C. H.; Kramer, P. L.; Yamada, S. A.; Nishida, J.; Tamimi, A.; Fayer, M. D. Carbon Dioxide in an Ionic Liquid: Structural and Rotational Dynamics. *J. Chem. Phys.* **2016,** *144* 104506.

27. Kramer, P. L.; Nishida, J.; Fayer, M. D. Separation of Experimental 2D IR Frequency-Frequency Correlation Functions into Structural and Reorientation-Induced Contributions. *J. Chem. Phys.* **2015,** *143* 124505.
28. Kramer, P. L.; Nishida, J.; Giammanco, C. H.; Tamimi, A.; Fayer, M. D. Observation and Theory of Reorientation-Induced Spectral Diffusion in Polarization-Selective 2D IR Spectroscopy. *J. Chem. Phys.* **2015,** *142* 184505.